Numerical Methods in Civil Engineering, 7-2 (2022) 16-32

Numerical Methods in Civil Engineering

Journal Homepage: https://nmce.kntu.ac.ir/

Comparison of seismic fragility of special moment frames in recent editions of ASCE 7 and ACI 318 regulations

Farhad Behnamfar*, Hamed Fazili Nezhad**

ARTICLE INFO

RESEARCH PAPER

Article history:
Received:
October 2021.
Revised:
May 2022
Accepted:
May 2022.

Keywords:
Seismic fragility, Special moment frames, ACI 318-99; ACI 318-05, ACI 318-11

Abstract:

The seismic safety levels provided by the three most recent editions of ACI and ASCE regulations for new moment frame structures are determined. Five special RC moment frames having 3, 5, 10, 15, and 20 stories are designed separately based on ACI 318-99, ACI 318-05, and ACI 318-11, and the associated seismic regulations of UBC 97, ASCE 7-05, and ASCE 7-10. A suit of 10 consistent earthquake records is selected for non-linear dynamic analysis of buildings. Incremental dynamic analysis is conducted, and the corresponding fragility curves are calculated. The comparison of results shows that seismic safety of special moment frame buildings has considerably improved from ACI 318-99 to ACI 318-11, and from UBC 97 to ASCE 7-10, owing its larger part to the improvements made in the two latter versions of the mentioned building codes. However, the safety enhancement is not uniform and is much less for buildings with larger fundamental periods, especially for periods larger than 1.0 sec. For structures with fundamental periods smaller than 1 sec, the collapse ratio has increased up to more than 70%. For larger fundamental periods, the increase is less than 20%. Changes in ASCE7 with regard to the R-factor and coefficients of the load combination equations and its introduction of stricter requirements for the allowable story drift are pinpointed to be the most important factors. For the ACI codes, stricter requirements regarding the confinement of the plastic hinges and configuration of the longitudinal reinforcement are recognized to be the most influential changes.

1. Introduction

Structural design codes and seismic design regulations are revised every several years to reflect the advances in knowledge and provide for improved safety of buildings. For example, the ACI 318 code, in its three most recent editions, was revised in 1999, 2005, and 2011, namely, every six years [1-3]. In parallel, the associated regulations for seismic loading, contained up to 1997 in UBC and afterwards in ASCE7, were revised in 1997 [4], 2005 [5], and 2010 [6]. The parallel evolution of loading, analysis, and design regulations is anticipated to result in seismically safer buildings.

Seismic safety, as a challenging concept, can be quantified by determining the probability of collapse for a certain intensity measure. In FEMA P695, a specific methodology is presented for determining seismic safety by calculating the fragility curve of the building under study as the probability of collapse versus the spectral acceleration at the fundamental period of the same building [7]. The computational procedure for arriving at such a fragility curve is the incremental dynamic analysis (IDA), in which the peak non-linear structural response is calculated several times under an earthquake record, each time amplified by a certain factor. Since the publication of FEMA P695 in 2009, a number of research works have been accomplished on the performance of reinforced concrete (RC) moment frames against collapse. Part of the above works focused on fragility using a certain assumption for the definition of collapse, and the other part focused on the definition of collapse itself. As representative examples, the first and second references belong to the first and other references to the second group. Richard et al. investigated the seismic

* *Corresponding author: Professor, Department of Civil Engineering, Isfahan University of Technology, Isfahan, Iran. E-mail: farhad@iut.ac.ir.*

** *Senior structural engineer, Isfahan, Iran.*

performance of intermediate RC moment frames in intermediate seismic zones [8]. Four and six-story frames were designed based on ACI 318-08 and evaluated based on FEMA P695 methodology. It was concluded that the seismic fragility of such frames was reduced to an acceptable level after the 2005 regulation. At the same time, an existing vulnerability against shear fracture was pinpointed, warranting further research. Yi et al. conducted an experimental study to investigate the capacity of RC frames against collapse [9]. A four-story frame having three bays was studied. The tendency for the collapse was prepared by removing an interior column in the first story. It was shown that the ultimate capacity of the frame calculated based on the plastic limit state is only about 70% of the collapse capacity of the frame in the experiment. Ibarra et al. studied the collapse capacity of structural frames using IDA analysis [10]. The global instability of the structure was selected as the criterion for collapse. It was concluded that the post-capping stiffness and displacement capacity were the two most decisive parameters in the collapse capacity determination of such systems, with P-Δ accelerating the collapse process.

Haselton and Deierlein investigated the seismic safety of modern buildings consisting of concrete special moment frames, including uncertainties in modeling and design [11]. Results of experiments on 255 columns were used for calibration and simulation of failure modes. The study showed that the plastic rotation capacity of concrete elements was larger than what is recognized by seismic design documents like FEMA356. Furthermore, the study showed that the height and type of the frames were less decisive in estimating the ultimate performance of the structures compared with uncertainty parameters and spectral shape. A study on the collapse behavior of steel special moment frames following the theoretical procedure of FEMA P695 was accomplished by Zareian et al. [12]. In this study, 3-bay frames with 1 to 20 stories were designed based on ASCE7-05 and AISC 341-05. For evaluation of the same buildings, their non-linear models were developed based on recent developments, and spectral accelerations were calculated at collapse. It was concluded that the special frames generally provided an acceptable margin of safety against collapse except for tall buildings in regions with high seismicity. El Howary and Mehanny [13] focused on multi-level seismic vulnerability assessment of reinforced concrete moment frame buildings and applied their results in the comparative design of two 4-story and 8-story buildings adopting both space- and perimeter-framed approaches. The buildings were dimensioned as per the seismic design code of Egypt. Using the IDA analyses, the fragility curves of the frames were calculated at different performance levels. The mean annual probabilities of exceeding various performance levels were then computed. Using the data generated, they evaluated the efficacy of the design code regulations in maintaining the desired levels of seismic performance. Masi et al. [14] developed the fragility curves of RC buildings designed only for gravity loads using non-linear dynamic analysis. The varying parameters included building age, number of stories, presence and position of infill panels, plan dimensions, external beams stiffness, and concrete strength.

Soltangharaei et al. employed the incremental dynamic analysis to derive the fragility curves of buckling restrained braced frames under near- and far-fault ground motions [15]. It was concluded that the seismic performance of the buckling restrained braced frames against near-fault records was similar to special moment frames or even better in some cases. Li et al. constructed a collapse ductility spectrum for concentrically braced frames considering the P-Δ effect and sudden loss in strength and stiffness. By plotting the collapse ductility and the ductility demand spectra on the same plane, they figured out the threshold period and the design ductility region for structural design [16]. Surana et al. conducted the incremental dynamic analyses for a number of low to mid-rise reinforced-concrete special moment frame buildings, non-conforming and conforming to the strong-column weak-beam design criterion. It was observed that abiding by the mentioned criterion leads to a significant reduction in collapse probability, especially for mid-rise buildings [17].

Speicher et al. presented the results of the collapse assessment of four steel special moment frames. Effects of modeling assumptions, including the utilization of the default ASCE 41 backbone curves versus experimentally-derived backbone curves, were studied. Generally, it was concluded that the performance indicated by an ASCE 41 assessment was conservative relative to the collapse performance indicated by a FEMA P695 assessment [18]. Farahbakhshtooli and Bhowmick presented a new strength deterioration model for stiffened infill plates to evaluate the seismic performance of stiffened steel plate shear walls using the FEMA P695 procedure. Static pushover and incremental dynamic analyses were conducted using 44 ground motions compatible to Western Canada. It was shown that the currently recommended seismic response modification factor, ductility-related force modification factor, and overstrength-related force modification factor for unstiffened steel shear walls could also be used to design the stiffened ones [19]. Kalantari and Roohbakhsh introduced the fragility curves of code-conforming reinforced concrete moment resisting frames under an aftershock [20]. Twenty recorded ground motion sequences, each including two seismic events, were utilized for non-linear incremental dynamic analysis. Maximum inter-story drift was employed as a damage index, and it

was shown that the probability of failure might differ due to the effects of a first event scenario, under a second one.
Kassem et al. studied the seismic behavior of ten types of six-story moment-resisting concrete frames, including one regular and nine setback frames with different configurations. Incremental dynamics analysis was performed under three sets of repeated ground motion records, and the maximum inter-story drift and the plastic hinge rotations were determined. The regular frame showed the lowest probability of failure [21]. Trapani and Malavisi evaluated the seismic fragility and residual capacity of masonry infilled reinforced concrete frames subject to mainshock/aftershock sequences. A double incremental dynamic analysis approach was used based on the combination of a mainshock signal at different intensities with a set of spectrum-compatible aftershocks scaled in amplitude with respect to the peak ground acceleration [22]. Intact and aftershock fragility curves were obtained by simulating seismic response with and without infills through a fully fiber section model developed in OpenSees. It was shown that masonry infills could drastically reduce the seismic fragility of RC frame structures during the main event and afterwards for mid-low intensity earthquakes depending on the capacity of RC members to support additional shear demands. Fattahi and Gholizadeh assessed the seismic performance of optimally designed steel moment frames in three phases, including optimization to meet the performance requirements, derivation of the fragility curves, and generation of the fragility curves for different damage levels [23].
Sotoudeh et al. [24] developed four limit states to be used in seismic performance evaluation of massive concrete dams using incremental dynamic analysis. It was applied to an integrated dam-reservoir finite-element model and was used to assess the probabilistic performance of the Pine Flat dam. Bakhshi and Soltanieh [25] presented the analytical fragility curves for a set of existing 3 to 6-story residential steel buildings with concentrically braced frames. They concluded that the seismic vulnerability of the mentioned structures generally increased as the number of stories became larger. The concentration of plastic behavior was also found to be mainly at the first-story levels of the buildings.
Jin and Gong performed the seismic capacity assessment and fragility analysis of existing containment structures subjected to near-fault ground motions. The incremental dynamic analysis was conducted, and three damage levels were proposed. It was found that the bottom location of the containment structure was prone to bending cracks, and the lower part of the structure was governed by diagonal shear cracks [26]. Hashmi and Madan studied the seismic fragility of masonry-infilled reinforced concrete frames. Various layout patterns for infill panels were considered along the height of the frames. The non-linear dynamic analysis was performed under forty near-field ground motions, and the peak inter-story drift, residual drift, and damage index were calculated. The generated data were used to develop seismic fragility curves for the generic medium-rise RC frames [27].
Special RC moment frames are one of the obligatory options in high seismicity regions. As it appears, the number of research studies on the collapse of special RC structures is relatively small. On the other hand, comparative studies on how the seismic fragility of such frames has decreased due to code improvements in recent years could be illuminating. Building design codes are revised every several years. It is expected that the newer versions provide for an enhanced safety level. With this perception, this study evaluates the level of safety in recent versions of ACI318 against collapse in a seismic event. Reinforced concrete moment frames are designed according to 99, 05, and 11 versions and are assessed based on FEMA P695. As a result, it can be judged how the advancement of knowledge on seismic safety has been reflected in newer versions of the code and how this reflection has been successful in enhancing safety.

2. Highlights Of The Seismic Design Regulations

This section presents a quick glance at the seismic design codes used in this study.

2.1 ACI 318-99 and UBC 97

ACI 318-99 was conjoined with UBC 97 for seismic design. A summary of the seismic regulations of UBC 97, contained in its sixth chapter, is followed.
Seismic zoning:
Six seismic zones, ordered from low seismicity to high seismicity, are introduced. In this paper, a pilot location is selected in California, which has very high seismicity.
Calculation of the base shear:
In UBC 97, base shear is calculated using Eq. (1):

$$V = \frac{C_V I}{RT} W \tag{1}$$

Where R is the response modification factor given in Table 16-N of the code, W is the effective seismic weight of the building, I is the importance factor based on usage, T is the fundamental period, and C_v is a spectral factor depending on seismicity and soil type, given in Table 16-R of the code.

2.1.1 The design spectrum

The design acceleration spectrum of UBC 97 is given in Figure 1.

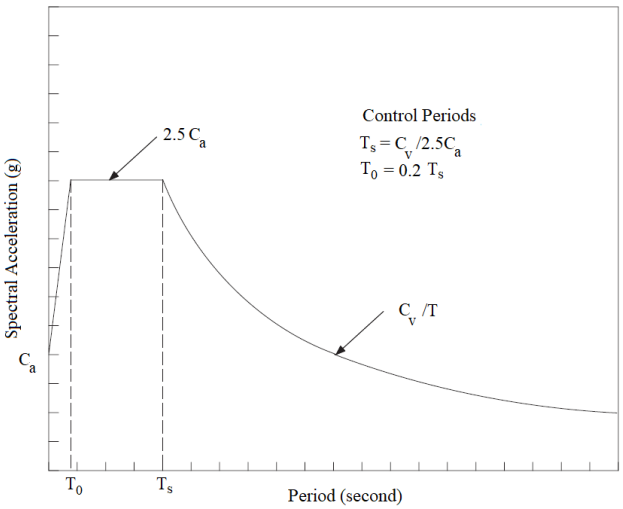

Fig. 1: Design acceleration spectrum of UBC 97

In Figure 1, C_a is a spectral shape factor given in Table 16-Q of the code varying with the seismicity and soil type of the region and T_0 and T_S are controlling periods introduced in the figure.

2.1.2 Load combinations of ACI 318-99

Part of the load combinations in ACI 318-99 pertaining to seismic forces are as follows:

$$\begin{aligned} &(1.2+0.5C_a I)DL+LL\pm E_{x,y}\\ &(0.9\pm 0.2)DL\pm E_{x,y}\\ &1.2DL+LL\pm \Omega_0 E_{x,y}\\ &0.9DL\pm \Omega_0 E_{x,y} \end{aligned} \qquad (2)$$

where DL and LL are the dead and live loads, respectively, $E_{x,y}$ is the seismic load along x and y directions, and Ω_0 is the over strength factor given in Table 16-N of UBC 97.

2.1.3 Check for lateral displacements

The checking equations are:

$$\begin{aligned} &\Delta_S \le \frac{0.025h}{0.7R} && T \le 0.7\sec\\ &\Delta_S \le \frac{0.02h}{0.7R} && T > 0.7\sec \end{aligned} \qquad (3)$$

in which Δ_S is story drift and h is the floor-to-floor story height.

2.1.4 Spectrum analysis

According to UBC 97, when doing a spectral analysis, the spectral base shear calculated as a combination of the modes exciting at least 90% of the seismic weight must be modified with regard to the base shear given in Equation (1).

For regular and irregular buildings, the spectral base shear must be at least 90% and 100% of the base shear of Equation (1), respectively.

2.2 ACI 318-05 (11) and ASCE 7-05 (10)

Seismic regulations in ACI 318-05 and ACI 318-11, and in association, ASCE 7-05 and ASCE 7-10, have many similarities and are reviewed here in the same section.

2.2.1 The base shear

According to ASCE 7-05 and ASCE 7-10, the base shear is calculated from Equation (4):

$$V = C_s W \qquad (4)$$

where C_s is the seismic response factor given in Equation (5):

$$\begin{aligned} C_s &= \frac{S_{DS}}{(\frac{R}{I})}(0.4+0.6\frac{T}{T_0}) && T \le T_0\\ C_s &= \frac{S_{DS}}{(\frac{R}{I})} && T_0 < T \le T_S\\ C_s &= \frac{S_{D1}}{T(\frac{R}{I})} && T_S < T \le T_L\\ C_s &= \frac{S_{D1}T_L}{T^2(\frac{R}{I})^2} && T > T_L \end{aligned} \qquad (5)$$

In Equation (5), S_{DS} and S_{D1} are the spectral response parameters at low periods and at a period of 1 sec, respectively. T_L is the transition period for long periods. S_{DS} and S_{D1} depend on the spectral accelerations at the corresponding periods on the bedrock (as a function of seismicity of the region) and the soil type. Six soil types, A to F, are introduced in ASCE in descending order of soil stiffness.

2.2.2 The design spectrum

In ASCE7, the design spectrum is as shown in Figure 2.

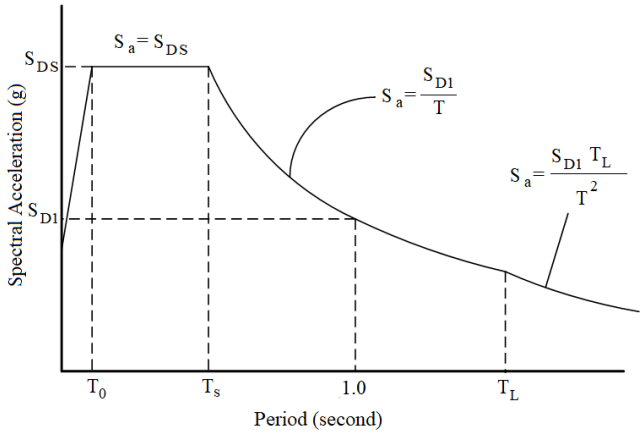

Fig. 2: The design spectrum of ASCE7

In Figure 2, T_0 and T_S are calculated using Equation (6):

$$T_0 = 0.2\frac{S_{D1}}{S_{DS}} \qquad (6\text{-a})$$

$$T_S = \frac{S_{D1}}{S_{DS}} \quad (6\text{-b})$$

2.2.3 Seismic design category

The occupancy importance of a building and the seismicity of the region in which it is located are combined in a unified subject called the seismic design category (SDC). Six SDCs, namely, A to F, are introduced in ascending order of importance and seismicity.

2.2.4 Load combinations

The seismic load combinations of ACI 318-05 and ACI 318-11 are as follows:

$$\begin{aligned} &(1.2+0.2S_{DS})DL + LL \pm \rho E_{x,y} \\ &(0.9-0.2S_{DS})DL \pm \rho E_{x,y} \\ &(1.2+0.2S_{DS})DL + LL \pm \Omega_0 E_{x,y} \\ &(0.9-0.2S_{DS})DL \pm \Omega_0 E_{x,y} \end{aligned} \quad (7)$$

where ρ is the redundancy factor, generally considered 1.3 for low redundancy buildings and 1.0 otherwise.

2.2.5 Check for drift

The actual drift of each story, δ_x , is calculated using Equation (8):

$$\delta_x = \frac{C_d \delta_{xe}}{I} \quad (8)$$

where δ_{xe} is the drift computed using the distribution of the base shear of Eq. (4) along height, and C_d is a displacement modification factor.

Then, δ_x must not exceed the acceptable values ascertained in the code based on the importance and structural system of the building. The acceptable values differ between 0.007 and 0.025 of the floor-to-floor height.

2.2.6 The spectral analysis

For regular and irregular buildings, the combined spectral base shear must not be less than 85% of the base shear of Equation (4).

According to ASCE 7-10, if the combined spectral base shear is less than $0.85C_SW$, δx must be modified by a factor equal to the ratio of the static base shear (Equation 4) to the combined spectral base shear. In the above regulation, C_S is equal to $0.5S_1/(R/I)$, in which S1 is the spectral acceleration at the period of 1 sec on the bedrock for the maximum considered earthquake.

Overall, the main differences between the building codes cited could be listed as presented in Table 1.

Table 1: the main differences between the building codes. (a) UBC and ASCE. (b) ACI.

UBC and ASCE	Base shear equation	R-factor	Load combination equations	Allowable story drift
UBC97	$V = \frac{C_v I}{RT} W$	8.5	1.4 DL 1.2 DL + 1.6 LL (1.2 + 0.5C_a I) DL + LL ± $E_{x,y}$ (0.9 ± 0.2) DL ± $E_{x,y}$ 1.2 DL + LL ±Ω_0 $E_{x,y}$ 0.9 DL ±Ω_0 $E_{x,y}$	$\Delta_s = \frac{0.025}{0.7R} = \frac{0.025 \times 300}{0.7 \times 8.5} = 1.26$ cm
ASCE7-05	$V = C_s W$	8	1.4 DL 1.2 DL + 1.6 LL (1.2+0.2S_{DS}) DL + LL ±ρ $E_{x,y}$ (0.9 - 0.2S_{DS}) DL ±ρ $E_{x,y}$ (1.2+0.2S_{DS}) DL ±Ω_0 $E_{x,y}$ + LL (0.9 – 0.2 S_{DS}) DL ±Ω_0 $E_{x,y}$	$\delta_{xe} = \frac{0.02 h_{sx} I}{C_d} = \frac{0.02 \times 300 \times 1}{5.5} = 1.09$ cm
ASCE7-05	$V = C_s W$	8	1.4 DL 1.2 DL + 1.6 LL (1.2+0.2S_{DS}) DL + LL ±ρ $E_{x,y}$ (0.9 - 0.2S_{DS}) DL ±ρ $E_{x,y}$ (1.2+0.2S_{DS}) DL ±Ω_0 $E_{x,y}$ + LL (0.9 – 0.2 S_{DS}) DL ±Ω_0 $E_{x,y}$	$\delta_{xe} = \frac{0.02 h_{sx} I}{C_d} = \frac{0.02 \times 300 \times 1}{5.5} = 1.09$ cm

3. The Buildings Studied

For the purposes of this study, five buildings consisting of special RC frames are designed using Etabs 9.4 according to three different code combinations of ACI 318-99 with UBC 97, ACI 318-05 with ASCE 7-05, and ACI 318-11 with ASCE 7-10. Each building consists of four parallel

frames both ways at equal bay spans of 196.85 in. (5 m). The floor-to-floor height is equally 118.11 in. (3 m).

The dead and live loads are assumed to be 6 kN/m^2 and 2 kN/m^2, respectively.

The location is the city of San Francisco in California, a place with very high seismicity. The soil type is C, being a medium stiff soil.

Based on the above assumptions, the spectrum parameters for UBC 97 are C_a = 0.4, C_v = 0.56, and Z = 0.4, where Z is the seismic zonation factor.

For ASCE 7-05 and ASCE 7-10, SDS = 1 and SD1 = 0.61, SDC = D.

Figure 3 shows the design spectra of UBC 97, ASCE 7-05, and ASCE 7-10 for the region.

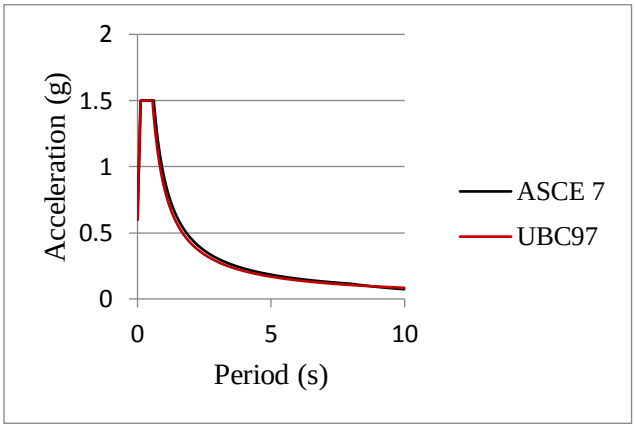

Fig. 3: The design spectra

Values of the design base shear of the studied buildings are calculated using Figure 3. They are mentioned in Table 2.

Table 2: Values of the design base shear, kN.

Building	UBC 97	ASCE 7-05	ASCE 7-11
3-story	665	704	704
5-story	1168	1235	1235
10-story	1520	1534	1534
15-story	1701	1716	1716
20-story	1867	1933	1933

Tables 3-7 show the results of structural design according to the above codes.

Table 3: Results of design for the 3-story building

Story	ACI 318-99			
	Exterior Column		Interior Column	
	Dims. (cm)	Rebar area (cm^2)	Dims. (cm)	Rebar area (cm^2)
1	30x30	21.91	35x35	18.78
2	30x30	18.76	35x35	13.4
3	30x30	24.71	35x35	9
ACI 318-05				
1	30x30	22.62	35x35	30.27
2	30x30	25.08	30x30	14.03
3	30x30	27.23	30x30	9
ACI 318-11				
1	30x30	23.8	35x35	31.4
2	30x30	26.01	30x30	15.56
3	30x30	28.04	30x30	9

Table 4: Results of design for the 5-story building

Story	ACI 318-99			
	Exterior Column		Interior Column	
	Dims. (cm)	Rebar area (cm^2)	Dims. (cm)	Rebar area (cm^2)
1	35x35	13.41	40x40	21.99
2	35x35	20.5	35x35	20.46
3	35x35	15.18	35x35	18.04
4	35x35	18.29	30x30	13.78
5	35x35	23.95	30x30	9
ACI 318-05				
1	35x35	22.22	40x40	37.91
2	35x35	29.05	35x35	35.57
3	35x35	23.76	30x30	26.64
4	30x30	21.07	30x30	20.19
5	30x30	28.27	30x30	9
ACI 318-11				
1	35x35	23.68	40x40	39.03

2	35x35	30.53	35x35	36.01
3	35x35	24.21	30x30	27.24
4	30x30	22.33	30x30	17.77
5	30x30	28.83	30x30	9

Table 5: Results of design for the 10-story building

Story	ACI 318-99			
	Exterior Column		Interior Column	
	Dims. (cm)	Rebar area (cm^2)	Dims. (cm)	Rebar area (cm^2)
1	40x40	28.519	45x45	51.95
2	40x40	21.05	45x45	32.11
3	40x40	20	40x40	46.09
4	35x35	28.6	40x40	38.74
5	35x35	24.07	40x40	19.71
6	35x35	23.65	35x35	30.02
7	35x35	15.52	35x35	18.76
8	35x35	20.26	30x30	17.9
9	35x35	13.12	30x30	9.44
10	35x35	23.31	30x30	9
ACI 318-05				
1	45x45	28.29	50x50	48.15
2	40x40	39.79	45x45	51.69
3	40x40	24.56	45x45	31.19
4	40x40	18.12	40x40	41.61
5	40x40	16.19	40x40	31.08
6	35x35	20.63	40x40	19.87
7	35x35	21.66	35x35	19.08
8	35x35	21.67	30x30	19.99
9	30x30	13.69	30x30	9
10	30x30	26.75	30x30	9
ACI 318-11				
1	45x45	29.76	50x50	48.42
2	40x40	40.58	45x45	51.78
3	40x40	26.18	45x45	32.45
4	40x40	20.04	40x40	42.28
5	40x40	18.16	40x40	32.51
6	35x35	22.01	40x40	21.89
7	35x35	22.93	35x35	21
8	35x35	22.57	30x30	22.1
9	30x30	14.73	30x30	9
10	30x30	27.39	30x30	9

Table 6: Results of design for the 15-story building

Story	ACI 318-99			
	Exterior Column		Interior Column	
	Dims. (cm)	Rebar area (cm^2)	Dims. (cm)	Rebar area (cm^2)
1	45x45	58.71	55x55	76.93
2	45x45	42.7	55x55	49.88
3	45x45	33.63	50x50	64.84
4	45x45	24.15	50x50	45.84
5	40x40	42.13	50x50	30.54
6	40x40	42.86	45x45	49.63
7	40x40	28.38	45x45	35.88
8	40x40	18.32	45x45	22.73
9	40x40	20.86	40x40	38.94
10	35x35	30.58	40x40	31.64
11	35x35	25.82	40x40	16
12	35x35	24.88	35x35	23.7
13	35x35	21.18	35x35	15.8
14	35x35	21.93	30x30	15.58
15	35x35	26.02	30x30	12.19
ACI 318-05				
1	50x50	57.44	60x60	76.17
2	50x50	39.67	55x55	69.24
3	45x45	49.99	55x55	49.46
4	45x45	42.69	50x50	66.94
5	45x45	26.06	50x50	46.47
6	40x40	45.23	50x50	34.74
7	40x40	43.85	45x45	48.12
8	40x40	25.03	45x45	31.04
9	40x40	24.65	40x40	41.76
10	35x35	33.79	40x40	34.42
11	35x35	34.71	40x40	16.3
12	35x35	27.07	35x35	19.7
13	35x35	19.35	35x35	12.25
14	35x35	12.6	30x30	9
15	35x35	21.34	30x30	9
ACI 318-11				
1	50x50	55.27	60x60	76.32

2	50x50	39.51	55x55	69.47
3	45x45	48.32	55x55	49.49
4	45x45	42.35	50x50	67.09
5	45x45	27	50x50	46.7
6	40x40	44.52	50x50	34.77
7	40x40	43.4	45x4	48.27
8	40x40	26.16	45x45	31.27
9	40x40	25.44	40x40	41.79
10	35x35	33.93	40x40	34.57
11	35x35	34.95	40x40	16.53
12	35x35	28.1	35x35	19.73
13	35x35	20.59	35x35	12.5
14	35x35	13.33	30x30	9
15	35x35	20.66	30x30	9

Table 7: Results of design for the 20-story building

Story	ACI 318-99			
	Exterior Column		Interior Column	
	Dims. (cm)	Rebar area (cm^2)	Dims. (cm)	Rebar area (cm^2)
1	60x60	76.2	65x65	106.6
2	55x55	74.0	65x65	97.3
3	55x55	60.2	60x60	96.9
4	55x55	45.1	60x60	76.5
5	50x50	65.0	60x60	56.4
6	50x50	52.7	55x55	73.0
7	50x50	37.0	55x55	54.2
8	50x50	25.0	50x50	90.9
9	45x45	43.6	50x50	62.2
10	45x45	32.0	50x50	41.9
11	45x45	22.1	45x45	57.8
12	45x45	20.3	45x45	48.1
13	40x40	26.6	45x45	40.4
14	40x40	27.6	40x40	47.5
15	40x40	18.1	40x40	35.9
16	40x40	16.0	40x40	22.2
17	40x40	19.2	35x35	23.7
18	35x35	18.1	35x35	21.8
19	35x35	20.7	30x30	15.4
20	35x35	19.6	30x30	9.2
ACI 318-05				
1	60x60	102.6	65x65	127.5
2	55x55	99.4	65x65	87.7
3	55x55	82.3	60x60	100.1
4	55x55	68.5	60x60	89.3
5	50x50	81.5	60x60	69.5
6	50x50	70.2	55x55	88.1
7	50x50	58.5	55x55	80.5
8	45x45	69.7	55x55	59.3
9	45x45	59.7	50x50	76.8
10	45x45	44.6	50x50	67.9
11	45x45	25.5	50x50	44.6
12	45x45	20.3	45x45	55.6
13	40x40	33.2	45x45	58.5
14	40x40	24.1	45x45	33.3
15	40x40	21.3	40x40	39.8
16	40x40	16.0	40x40	21.5
17	35x35	20.5	40x40	18.7
18	35x35	21.3	35x35	16.4
19	35x35	12.3	30x30	12.9
20	35x35	16.5	30x30	9.0
ACI 318-11				
1	60x60	102.6	65x65	127.5
2	55x55	99.4	65x65	87.7

3	55x55	82.3	60x60	100.1
4	55x55	68.5	60x60	89.3
5	50x50	81.5	60x60	69.5
6	50x50	70.2	55x55	88.1
7	50x50	58.5	55x55	80.5
8	45x45	69.7	55x55	59.3
9	45x45	59.7	50x50	76.8
10	45x45	44.6	50x50	67.9
11	45x45	25.5	50x50	44.6
12	45x45	20.3	45x45	55.6
13	40x40	33.2	45x45	58.5
14	40x40	24.1	45x45	33.3
15	40x40	21.3	40x40	39.8
16	40x40	16.0	40x40	21.5
17	35x35	20.5	40x40	18.7
18	35x35	21.3	35x35	16.4
19	35x35	12.3	30x30	12.9
20	35x35	16.5	30x30	9.0

Tables 3-7 show that the reinforcement weight is considerably larger in newer versions of ACI. The difference is more tangible between ACI 318-99 and ACI 318-05. The seismic safety implications of this difference will be determined in the next sections. The fundamental periods of the 3 to 20-story buildings are respectively 0.48, 0.74, 1.39, 2, and 2.60 sec.

Based on the information in Tables 3-7, the change in the concrete volume and reinforcement weight can be calculated. Such a computations shows that volume of concrete of the 3, 5, 10, 15, and 20-story buildings increased from 1997 to 2010 versions by 0.1%, 1.0%, 1.8%, 3.7% and 5.4%, respectively. For the reinforcement, the increase is 4.7%, 3.4%, 2.2%, 1.7% and 6.4%, respectively for the same buildings.

Browsing the above tables shows a considerable difference between the design results. This difference partly relates to rounding the design outcome and making typical designs through a story and along successive stories, and partly to small differences between the design rules in different years. Nevertheless, the main reasons seem to be the larger design base shear in the newer versions of the building codes and putting more restrictions on story drifts in recent years. As seen in Table 2, the design base shear has increased by 5.9%, 5.7%, 1.0%, 1.0% and 3.5% for the 3, 5, 10, 15, and 20-story buildings from 1997 to 2010 versions. However, to a much greater extent, for the design drift, for example, for the 3-story building with a period of 0.48 sec, the maximum admissible drift in each story is calculated to be 1.26 and 1.09 cm according to UBC 97 and the two versions of ASCE, respectively, which shows a 14% reduction. Therefore, stricter drift limits seem to be the main cause, followed by larger base shear values.

4. Non-Linear Modeling For Seismic Evaluation

4.1 The software

Because of being convenient for IDA and having strong graphical capabilities, the software SeismoStruct V6.5 is selected for doing the numerical calculations of this study for collapse evaluation of the designed structures [28].

4.2 Modeling of steel

The stress-strain relation of steel rebars for non-linear modeling is selected as the one suggested by OpenSees as steel02 [29]. It is shown schematically in Figure 4.

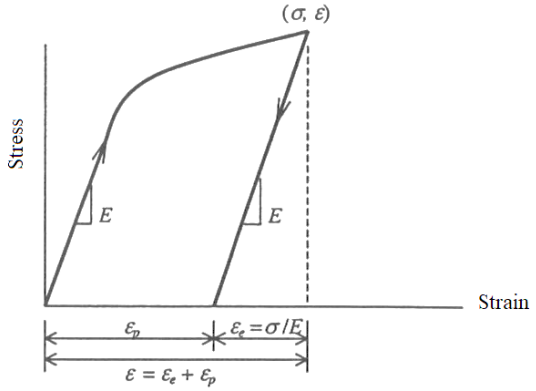

Fig. 4: The stress-strain relation of steel [29].

In Figure 4, ES is the modulus of elasticity, Fy is the yield stress, μ is the strain hardening parameter, R_0 is the transition curve's initial shape parameter, a_1 and a_2 are calibration factors for the shape of the transition curve, a_3 and a_4 are calibration factors for isotropic hardening, and ε_{ult} is the ultimate strain. Table 8 shows the values of the above parameters for a S400 steel assumed in this study [30].

Table 8: Values of the stress-strain parameters of the steel rebars

E_S (MPa)	F_y (MPa)	μ	R_0	a_1	a_2	a_3	a_4	ε_{ult}	Unit weight (kN/m^3)
200000	400	0.005	20	18.5	0.15	0	1	0.1	76.5

The use of the above constitutive model for steel is common because of its acceptable accuracy in the prediction of steel behavior as well as the fact that it makes a faster convergency in numerical analysis compared with more accurate models.

4.3 Modeling of concrete

The stress-strain relation of plain concrete is according to Mander et al. [31-35]. It is shown in Figure 5 with its parameters as illustrated in Table 9.

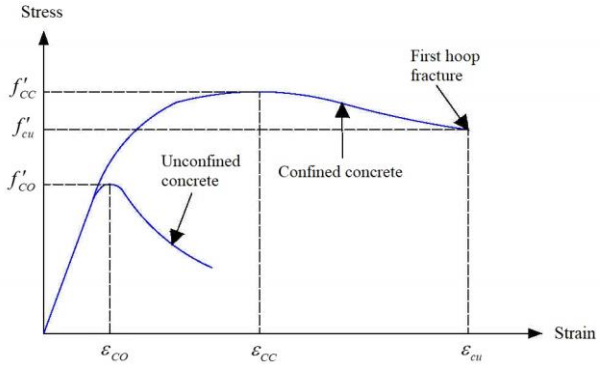

Fig. 5: The stress-strain relation of concrete.

Table 9: Values of the stress-strain parameters of concrete

Concrete type	f'_{CO} (MPa)	f_{yh} (MPa)	ε_{CO}	k_e	E_c (MPa)
Confined	28	300	0.002	1.2	26457.5
Unconfined	28	300	0.002	1	26457.5

4.4 The plastic hinges

Excessive seismic load results in the formation of plastic hinges at the member ends. This is simulated herein by modeling an elastic beam or column with concentrated plastic hinges at its ends. A plastic hinge is a zero-length rotational spring being elastic (as part of the beam) before yield.

For computational needs, a certain length is considered for the plastic hinge (not the non-linear spring). It is only used for converting curvature to rotation at the ends of members since the program calculates the curvature first but needs to follow the moment-rotation path at the zero-length non-linear end springs. Panagutakus and Fardis proposed the following equation for the calculation of the plastic hinge length based on tests of more than a thousand concrete members [36]:

$$L_P = 0.12z + 0.014 f_y d_b \quad (9)$$

In Eq. (9) L_P is the plastic hinge length, f_y and d_b are the yield stress and the diameter of the longitudinal rebars, and z is the distance between the critical section and the point of contraflexure.

z varies between 0.15 to 0.2 of the bay length (L) in practical cases. It is assumed to be 0.2L in this research.

Figure 6 shows the moment-rotation curve of plastic hinges of RC members.

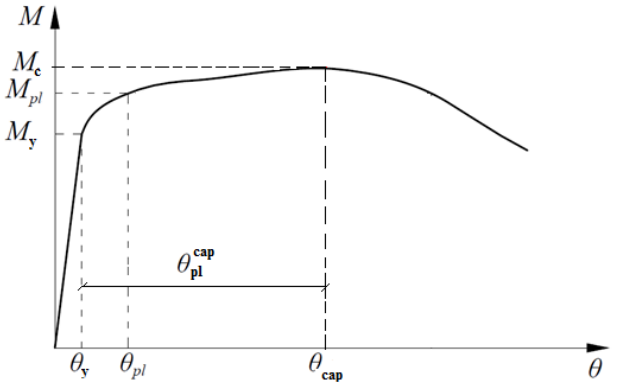

Fig. 6: The moment-rotation curve of the plastic hinges [37]

In Figure 6, θ_y is rotation at the yield moment (M_y), θ_{pl} is rotation at the plastic moment (M_{pl}), θ_{cap} is rotation at the maximum tolerated moment (M_c), and θ_{pl}^{cap} is shown in the figure. These parameters are characterized by the following equations:

$$\begin{aligned} \theta_{pl}^{cap} &= 0.13(1+0.55\alpha_{sl})(0.13)^{v}(0.02+40\rho_{sh})^{0.65}(0.57)^{0.01C_{units}} \\ \theta_{pl} &= (0.76)(0.31)^{v}(0.02+40\rho_{sh})^{1.02} \le 0.1 \\ \frac{M_c}{M_y} &= (1.25)(0.89)^{v}(0.91)^{0.01C_{units}f'_c} \end{aligned} \quad (10)$$

In Eq. (10), f'_c is the compressive strength of concrete, v is the axial force ratio equal to $P/(A_g.f'_c)$ where A_g is the cross section area and P is the axial force, ρ_{sh} is the transverse reinforcement ratio, α_{sl} is a factor taken to be unity where bond slip is possible, and C_{units} is unity when use is made of MPa units. An important point is the fact that the ductility capacity of a plastic hinge and the deformation needed for it to lose stiffness and reach the ultimate strength increase with ρ_{sh} according to Figure 6 and Eq. (10) for θ_{pl}^{cap}. As from 99 to 05 versions of ACI value of the confining transverse reinforcement has been increased considerably, it postpones the collapse of newer buildings proportionally.

5. The Earthquake Records

A suite of 10 earthquake records is selected for the IDA analysis. The number of records, i.e., 10, is assumed to be good enough for statistical calculations associated with IDA. Using at least 7 ground motions has been recommended by ASCE7-10 when averaging is purposed, like the calculations of IDA. For this purpose, the database of PEER NGA of strong ground motions is utilized [38]. The search criteria are as follows:

- Earthquake magnitude (M):
- Soil type C (a firm soil): 360 m/s < VS < 760 m/s, where VS is the shear wave velocity in soil.

- Distance to the causative fault (R): 20 km < R < 50 km

With the above criteria, a number of records are extracted. After examining the response spectrum of each record, 10 records with more similarity to the design spectra (UBC97 and ASCE7) are selected for the IDA analysis. Table 10 shows the characteristics of the selected earthquakes.

Table 10: The selected earthquakes

Record ID	NGA number	Earthquake name	Magnitude	Shear wave velocity (m/s)	Fault distance (km)
R1	0776	Loma Prieta	6.93	370.80	27.93
R2	0534	N. Palm Springs	6.06	370.80	23.31
R3	0288	Irpinia, Italy	6.90	500	22.56
R4	0974	Northridge	6.69	446	22.21
R5	1524	Chi-Chi, Taiwan	7.62	446.60	45.18
R6	0339	Coalinga	6.36	376.10	29.38
R7	1794	Hector Mine	7.13	379.30	31.06
R8	0033	Parkfield	6.19	527.90	24.76
R9	0057	San Fernando	6.61	450.30	22.63
R10	0587	New Zealand	6.60	424.80	20.42

In Figure 7, the response spectra of the selected earthquakes are shown along with two vertical lines corresponding to 0.2 T_{min} and 1.5 T_{max}, where T_{min} and T_{max} are fundamental periods of 3 and 20-story buildings. The coefficients 0.2 and 1.5 are for consideration of the effects of higher modes and lengthening of the fundamental period due to non-linear behavior. It should be noted that ASCE7 requires that the spectrum scaling of the set of ground motions be done in the interval 0.2-1.5T1, where T1 is the fundamental period of the building. However, such scaling is unnecessary in this research because the study is done using incremental dynamic analysis. In such an investigation, the records are scaled based on their PGA or Sa (spectral acceleration) and are changed to small earthquakes. They are next increased to gradually larger ones. Figure 7 is intended to provide only a visual comprehension of how the selected original records vary compared with the design spectrum in the period span of interest including all buildings.

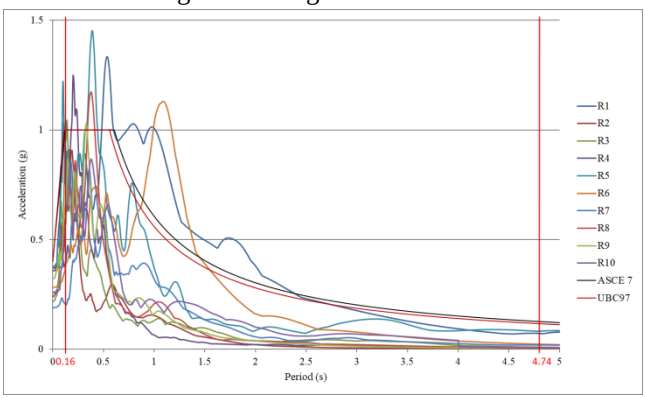

Fig. 7: Response spectra of the selected earthquakes

6. The Fragility Analysis

Certain steps are taken according to FEMA P695 to calculate the fragility curves and collapse safety level of the special RC frames under study as follows.

6.1 Calculation of the IDA curves

Figure 8 shows the IDA curve, for instance, for the 5-story building under record R2.

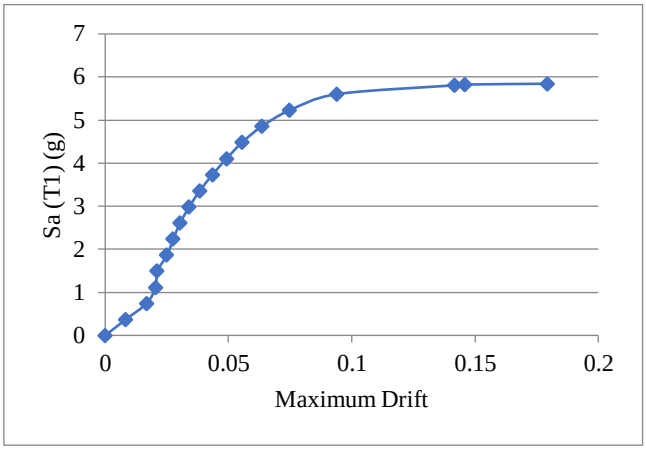

Fig. 8: The IDA curve of the 5-story building under earthquake R2, designed with ACI 318-99

The horizontal axis of Figure 8 shows the maximum inter-story drift ratio during the non-linear dynamic response along the height of the building. It is equal to the envelope of the maximum displacement of the roof of each story relative to its floor divided by the story height. The vertical axis shows the spectral acceleration, Sa, under each earthquake at the fundamental period of the building under study. According to Vamvatsikos and Cornell [39], for the calculation of an IDA curve, the original accelerogram of the earthquake each time is multiplied by a scale factor beginning from small values. The maximum drift ratio defined above is then calculated for the scaled record with the non-linear analysis of the building. The above spectral acceleration is also calculated using the response spectrum of the scaled record. This determines one point of an IDA

curve. The record is then scaled up, and the analysis is repeated until the structure collapses under a scaled earthquake for a certain scale factor.

Definition of collapse spectral acceleration is also important. It is generally associated with where the IDA curve flattens (a zero lateral stiffness), which is equivalent to dynamic instability. Such instability occurs at inter-story drift ratios as large as 10-20%. This is very important when choosing between non-linear dynamic analysis algorithms to select a procedure that does not prematurely diverge due to numerical problems. Otherwise, the collapse point is underestimated. On the other hand, the non-linear modeling of section behavior should include strength and stiffness degradation so as not to overestimate the collapse point [40]. Because the calculation of the collapse Sa is purposed, the definition of the collapse point does not affect the results sensibly. The reason behind this fact is that, as shown in Figs. 9 and 10, after a drift of about 15%, the IDA curve has flattened under all of the earthquakes utilized for the moment frames of this study. Therefore, taking the collapse drift to be a value larger than 15% does not affect the value of the collapse Sa. On the other hand, most non-linear structural programs cannot converge after drifts as large as values more than 20%. Therefore, to be sure, the program can be terminated at a drift of 20%, something that was followed in this study.

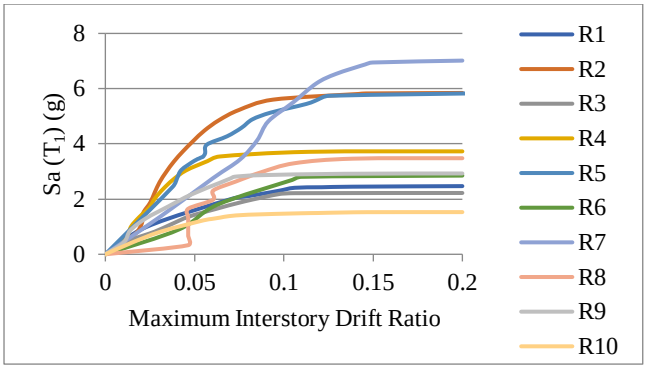

Fig. 9: The IDA curves of the 5-story building, designed with ACI 318-99

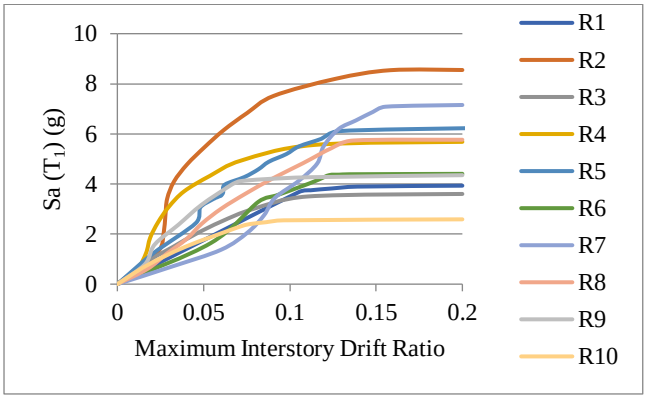

Fig. 10: The IDA curves of the 5-story building, designed with ACI 318-05

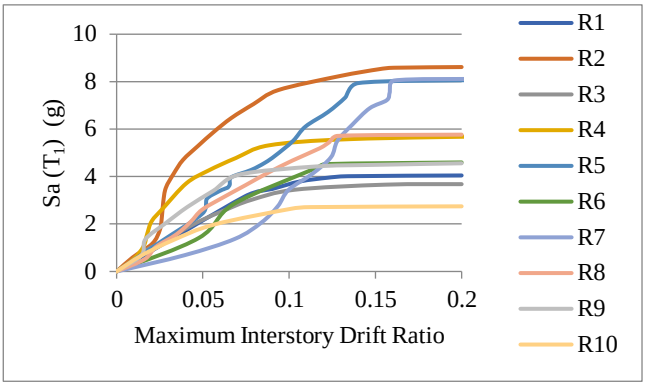

Fig. 11: The IDA curves of the 5-story building, designed with ACI 318-11

With the above points in mind, it can be said that according to Figure 8, the collapse Sa of the 5-story building under earthquake R2 is about 6 g, where g is the acceleration of gravity. This is while the same quantity is only about 1.5 g under earthquake R10, according to Figure 9. It shows how the collapse Sa can largely vary from one earthquake to another. Therefore, because of the importance of the frequency content of earthquakes, the collapse Sa cannot be judged upon under one single earthquake. Otherwise, it can be misleading to wrong conclusions. For instance, the IDA curves of the 5-story building designed with the three ACI versions subject to all earthquakes are shown in Figures. 9-11. According to these figures, while the collapse Sa for this building varies between 1.5-7g, it remains under 4g for the more populated part of the earthquake suit. As seen in Figure 7, at and near the fundamental period of the 5-story building, i.e., 0.7 sec, most of the response spectra behave similarly except those of two or three earthquakes. It shows that most of the records have similar frequency content for the important period range of this building. It is reflected similarly in the amplitudes of the IDA curves in Figs. 9-11 too.

6.2 Determination of fragility curves

The multiple IDA curves corresponding to a single building under different earthquakes give a distribution of collapse Sa's for the same building. Therefore, different properties of such a distribution can be calculated if a certain pattern is selected for the statistical distribution of data.

Shome et al. observed that a log-normal distribution has a better fit on the non-linear structural responses than other possible distributions [36]. A log-normal distribution is defined as a continuous function of the normal distribution of logarithmic variants. The log-normal probability distribution function (pdf) is defined as follows:

$$f(X;\mu,\sigma)=\frac{1}{X\sigma\sqrt{2\pi}}e^{-\frac{(\ln x-\mu)^2}{2\sigma^2}} \quad (11)$$

Integration of the above equation results in the cumulative distribution function (CDF) as follows:

$$P = F(X;\mu,\sigma) = \frac{1}{\sigma\sqrt{2\pi}}\int_0^x \frac{1}{t} e^{-\frac{(\ln t-\mu)^2}{2\sigma^2}} \quad (12)$$

It can be shown that Eq. (12) can conveniently be replaced with Eq. (13):

$$P(collapse / IM) = F(X;\mu,\sigma) = \phi(\frac{\ln X - \mu_{\ln x}}{\sigma_{\ln x}}) \quad (13)$$

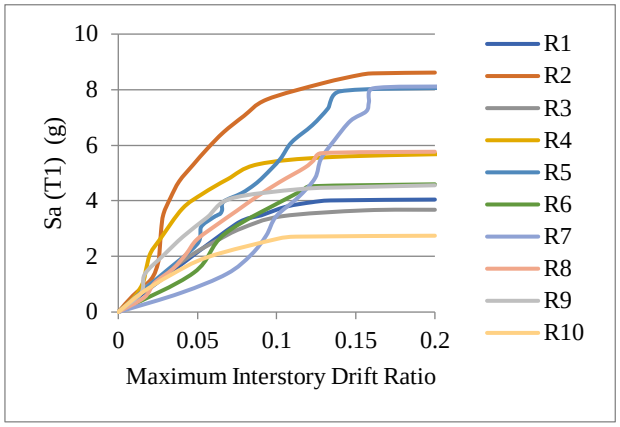

(a)

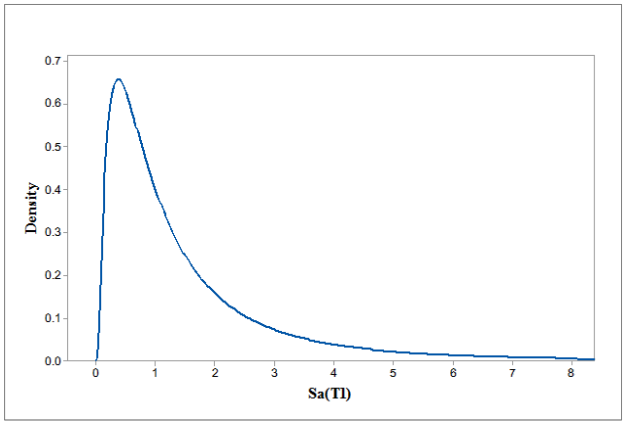

(b)

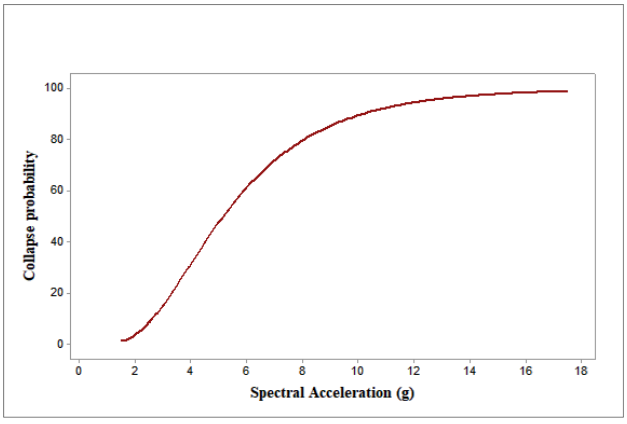

(c)

Fig. 12: The fragility analysis of the 5-story building designed with ACI 318-99. (a) The IDA curves. (b) The probability density function. (c) The fragility curve.

In the equations 11-13, μ and σ are the average and standard deviation of ,X and X is selected to be the collapse Sa. ϕ is the cumulative distribution function. Also, μ_{lnx} and σ_{lnx} are the average and standard deviation of ln x values and ln shows the natural logarithm. In calculating σ_{lnx} , only demand uncertainties are considered, while contributions from capacity and modeling uncertainties are ignored.

The average collapse spectral accelerations ($\mu_{\ln x}$) and their standard deviations ($\sigma_{\ln x}$)for the studied buildings are calculated using the IDA curves of Figures 9-11. It is shown again in part (a) of Figure 12. These parameters are used in Eqs. (11-13) to calculate each point of the fragility curves. For instance, the fragility curve corresponding to the IDA curves of Figure 9 is demonstrated in part (c) of Figure 12. Each point of part (c) of the figure corresponds to a collapse probability according to Eq. (13). The horizontal coordinate of those points represents the collapse spectral acceleration according to part (a) of the same figure.

Figure 12 shows the procedure of calculating the fragility curve of the 5-story building.

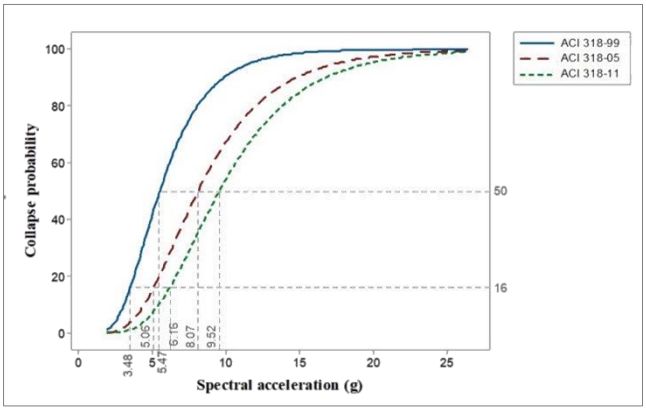

Fig. 13: The fragility curves of the 3-story building

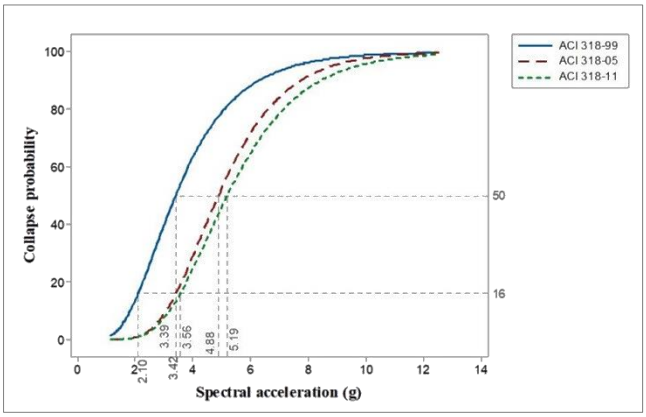

Fig. 14: The fragility curves of the 5-story building

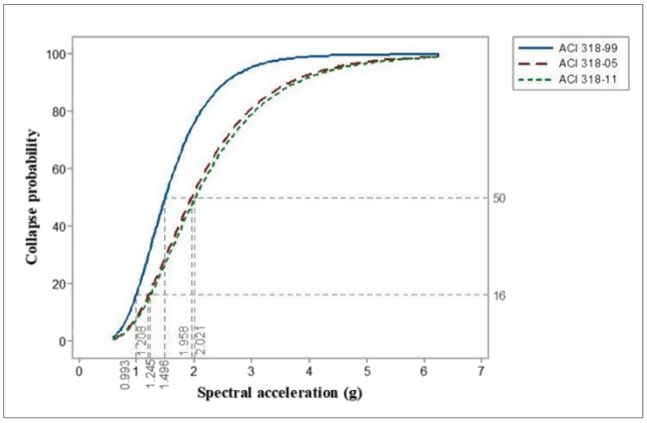

Fig. 15: The fragility curves of the 10-story building

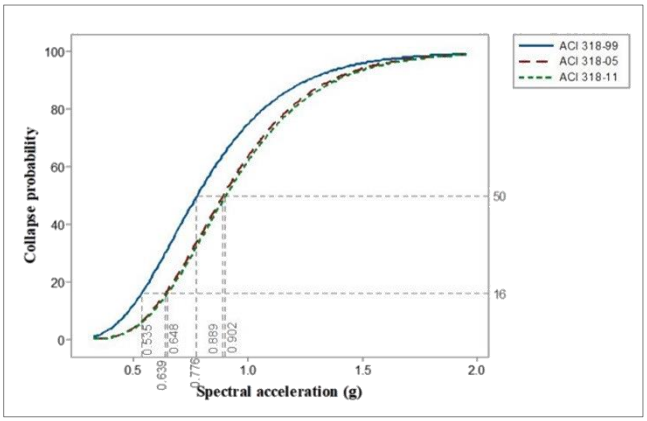

Fig. 16: The fragility curves of the 15-story building

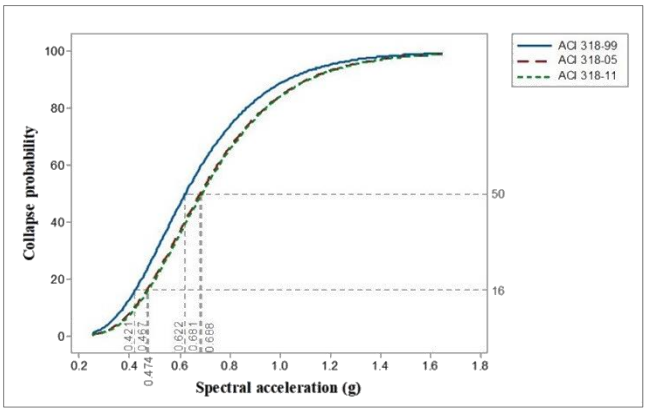

Fig. 17: The fragility curves of the 20-story building

Figures 13-17 show the fragility curves of all of the buildings. In each figure, three fragility curves corresponding to different versions of ACI are shown.

What is generally observed in Figs. 13-17 is that probability against a certain Sa has decreased from ACI 318-99 to ACI 318-05 up to 40% for periods less than 2 sec. This probability again decreased in ACI 318-11, but the reduction from ACI 318-05 to ACI 318-11 is much smaller and reaches a maximum value of about 10%.

6.3 Calculation of safety margin against collapse

The margin of safety against collapse is calculated as the ratio of a certain probability of collapse Sa to the Sa at the maximum considered earthquake (MCE) level, both calculated at a specific fundamental period. This is called the collapse margin ratio (CMR) value. The Sa's at the maximum considered earthquake (MCE) level are those with a probability of exceedance of 2% in 50 years (equivalent to a 2475-year return period). This is taken as 1.5 times the design Sa, which corresponds to a probability of exceedance of 10% in 50 years corresponding to a return period of 475 years.

Figures 18 and 19 show Sa(T1) at various periods based on different revisions of ACI for median (50 percentile) and average minus standard deviation (16 percentile) levels. For use with these figures, the fundamental period, T1, should be calculated using cracked member sections.

While both of figures 18 and 19 show a considerable increase in collapse safety from the 99 to 05 and then to 11 editions, CMR values corresponding to the 16 percentiles are about 60% smaller than those of the 50 percentiles. Moreover, the 50 percentile values seem to be safely large enough. Tables 11 and 12 show the 50 and 16 percentile CMR values, respectively, for different buildings and various editions of ACI.

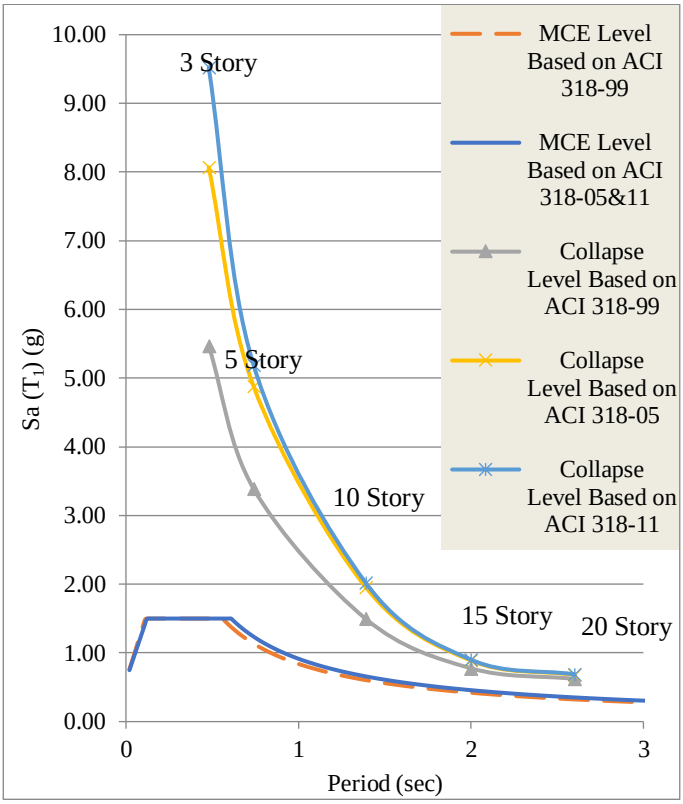

Fig. 18: Sa(T1) for the average (50 percentile) level

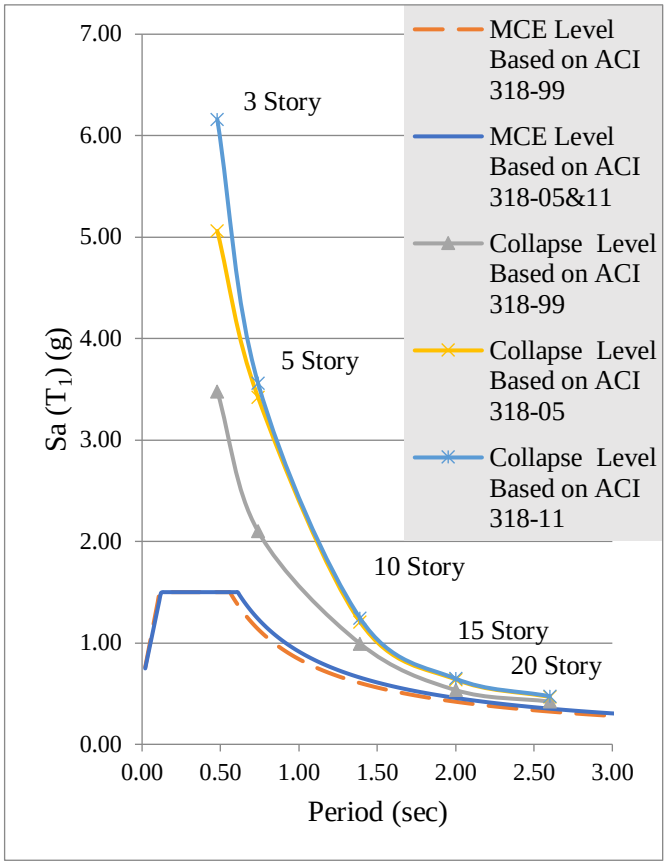

Fig. 19: Sa(T1) for the average minus standard deviation (16 percentile) level

Table 11: The 50 percentile CMR values.

Period (sec)	CMR		
	ACI 318-99	ACI 318-05	ACI 318-11
0.5	3.55	5.21	6.15
1	2.99	3.75	3.90
1.5	2.32	2.68	2.76
2	1.87	1.90	1.95
2.5	1.86	1.88	1.90

Table 12: The 16 percentile CMR values.

Period (sec)	CMR		
	ACI 318-99	ACI 318-05	ACI 318-11
0.5	2.33	3.43	4.13
1	1.94	2.61	2.63
1.5	1.55	1.66	1.67
2	1.38	1.56	1.56
2.5	1.29	1.43	1.43

According to Table 11, the CMR values vary from over 6 for low-rise (3-story) to about 2 for intermediate (20-story) buildings based on ACI 318-11. For the same cases, the CMR values vary between 4 and 1.3 in Table 12. Up to buildings with a fundamental period of 2 sec, the difference between CMR values of various ACI versions, especially between ACI 318-99 and the others, is considerable. From the 1.5 sec period upward, the difference diminishes. While the above results clearly show a considerable improvement against collapse in very strong MCE earthquakes, they show a non-uniform safety with a lower margin of safety for taller buildings. Determining the seismic safety level provided for high-rise buildings needs more extensive research. The reason for the CMR being much different for short and tall buildings can be related to the larger increase of the design base shear for shorter buildings. According to Figs. 18 and 19 that show variations of Sa with period, and what is mentioned at the end of Sec. 3, the base shear was increased by about 6% for the 3-story building, from UBC97 to ASCE7-10, while it was increased only by 3.5% for the 20-story building in the same time interval. It seems to be the main reason for the larger CMR values for the shorter buildings.

7. Conclusions

In this research, the fragility curves and the collapse safety margin factors were calculated by incremental dynamic analysis for RC special moment resisting frames designed based on three recent editions of ACI. There have been many changes in the related codes in the last 20 years. In comparison, the changes mostly responsible for the enhanced seismic behavior of the buildings following the newer versions of the codes seem to be as follows. In newer versions of the companion seismic codes, changes in the R-factor, the introduction of the coefficient of indeterminacy, and variations of the load combination formula are the most important factors. In the new ACI codes, improvement of the regulations for the confinement of the critical (plastic) zone and the minimum configuration of the longitudinal reinforcement have been the prime affecting changes.

The results showed that:

1. The safety against seismic collapse under very strong earthquakes has considerably increased from 99 to 05 revisions and, to a smaller extent, to the 11 revision of ACI.

2. The increase in safety is not uniform and becomes smaller as the fundamental period increases. From a 1.5 sec period upwards, the safety provided by the three versions is almost identical, and the factor of safety is only marginally over unity.

3. More stringent restrictions on the story drift limit and requirements for providing a larger volume of the transverse reinforcement in the plastic hinge regions were identified as the main reasons behind collapse safety enhancement in the newer versions of the code.

References

[1] American Concrete Institute and International Organization for Standardization. (1999). Building Code Requirements for Structural Concrete (ACI 318-99).

[2] American Concrete Institute and International Organization for Standardization. (2005). Building Code Requirements for Structural Concrete (ACI 318-05).

[3] American Concrete Institute and International Organization for Standardization (2011). Building Code Requirements for Structural Concrete (ACI 318-11).

[4] Uniform Building Code (UBC-97). (1997, April). Structural Engineering Design Provisions. International Conference of Building Officials, California, USA.

[5] American Society of Civil Engineers. (2005). Minimum Design Loads for Buildings And Other Structures (ASCE 7-05).

[6] American Society of Civil Engineers (2010). Minimum Design Loads for Buildings And Other Structures (ASCE 7-10).

[7] Applied Technology Council. (2009). Quantification of Building Seismic Performance Factors (FEMA P695).

[8] Richard, M. J., Albano, L. D., Kelly, D., & Liel, A. B. (2010). Case Study On The Seismic Performance of Reinforced Concrete Intermediate Moment Frames Using ACI Design Provisions. In Structures Congress 2010.

[9] Yi, W.J., He, Q.F., Xiao, Y., & Kunnath, S.K. (2008). Experimental Study on Progressive Collapse-Resistant Behavior of Reinforced Concrete Frame Structures. ACI Structural Journal, 105(4), 433-439.

[10] Ibarra, L.F., & Krawinkler, H. (2005). Global Collapse of Frame Structures under Seismic Excitations. Ph.D. Dissertation. Stanford University.

[11] Haselton, C.B., & Deierlein, G.G. (2007). Assessing Seismic Collapse Safety of Modern Reinforced Concrete Moment Frame Buildings. Ph.D. Dissertation. Department of Civil and Environmental Engineering, Stanford University.

[12] Zareian, F., Lignos, D. G., & Krawinkler, H. (2010). Evaluation of Seismic Collapse Performance of Steel Special Moment Resisting Frames Using FEMA P695 (ATC-63) Methodology. In Structures Congress 2010, (1275-1286).

[13] El Howary, H. A., & Mehanny, S. S. F. (2011). Seismic Vulnerability Evaluation of RC Moment Frame Buildings in Moderate Seismic Zones. Earthquake Engineering & Structural Dynamics, 40(2), 215-235.

[14] Masi, A., Digrisolo, A., & Manfredi, V. (2015). Fragility Curves of Gravity-Load Designed RC Buildings with Regularity in Plan. Earthquakes and Structures, 9(1), 1-27.

[15] Soltangharaei, V., Razi, M., & Vahdani, R. (2016). Seismic Fragility of Lateral Force Resisting Systems Under Near and Far-Fault Ground Motions. International Journal of Structural Engineering, 7(3), 291-303.

[16] Li, G., Dong, Z. Q., Li, H. N., & Yang, Y. B. (2017). Seismic Collapse Analysis of Concentrically-Braced Frames by the IDA Method. Advanced Steel Construction, 13(3), 273-292.

[17] Surana, M., Singh, Y., & Lang, D. H. (2018). Effect of Strong-Column Weak-Beam Design Provision on the Seismic Fragility of RC Frame Buildings. International Journal of Advanced Structural Engineering, 10(2), 131-141.

[18] Speicher, M.S., Dukes, J., & Wong, K.K. (2018, June). Using FEMA P695 to Interpret ASCE 41 Seismic Performance of Special Moment Frames. Eleventh U.S. National Conference on Earthquake Engineering, Los Angeles, USA.

[19] Farahbakhshtooli, A., & Bhowmick, A.K. (2019). Seismic Collapse Assessment of Stiffened Steel Plate Shear Walls Using FEMA P695 Methodology. Engineering Structures, 200, Article 109714.

[20] Kalantari, A., & Roohbakhsh, H. (2019). Expected Seismic Fragility of Code-Conforming RC Moment Resisting Frames Under Twin Seismic Events. Journal of Building Engineering, Article 101098.

[21] Kassem, M. M., Mohamed Nazri, F., Wei, L. J., Tan, C. G., Shahidan, S., & Mohd Zuki, S. S. (2019). Seismic Fragility Assessment for Moment-Resisting Concrete Frame with Setback Under Repeated Earthquakes. Asian Journal of Civil Engineering, 20(3), 465-477.

[22] Di Trapani, F., & Malavisi, M. (2019). Seismic Fragility Assessment of Infilled Frames Subject to Mainshock/Aftershock Sequences Using a Double Incremental Dynamic Analysis Approach. Bulletin of Earthquake Engineering, 17(1), 211-235.

[23] Fattahi, F., & Gholizadeh, S. (2019). Seismic Fragility Assessment of Optimally Designed Steel Moment Frames. Engineering Structures, 179, 37-51.

[24] Sotoudeh, M. A., Ghaemian, M., & Moghadam, A. S. (2019). Determination of Limit-States for Near-Fault Seismic Fragility Assessment of Concrete Gravity Dams. Scientia Iranica. Transaction A, Civil Engineering, 26(3), 1135-1155.

[25] Bakhshi, A., & Soltanieh, H. (2019). Development of Fragility Curves for Existing Residential Steel Buildings with Concentrically Braced Frames. Scientia Iranica, 26(4), 2212-2228.

[26] Jin, S., & Gong, J. (2020). Damage Performance Based Seismic Capacity and Fragility Analysis of Existing Concrete Containment Structure Subjected to Near Fault Ground motions. Nuclear Engineering and Design, 360, Article110478.

[27] Hashmi, A. K., & Madan, A. (2020). Fragility Analysis of Infilled Reinforced Concrete Frames Subjected to Near-Field Ground Motions. KSCE Journal of Civil Engineering, 24(1), 122-130.

[28] SeismoSoft. (2015). Earthquake Engineering Software Solutions. Pavia, Italy.

[29] Pacific Earthquake Engineering Research Center (PEER). (2015). Open System for Earthquake Engineering simulation.

[30] Zhang, G. (2006). Inelastic Modeling of Reinforcing Bars and Blind Analysis of The Benchmark Tests on Beam Column Joints Under Cyclic Loading. Master's Thesis. Rose School, European School for Advanced Studies in Reduction of Seismic Risk.

[31] Mander, J. B., Priestley, M. J., & Park, R. (1988). Theoretical Stress-Strain Model for Confined Concrete. Journal of Structural Engineering, 114(8), 1804-1826.

[32] Ho, J. C. M., Pam, H. J., Peng, J., & Wong, Y. L. (2011). Maximum Concrete Stress Developed in Unconfined Flexural RC Members. Computers and Concrete, 8(2), 207-227.

[33] Ergun, M., & Ates, S. (2013). Selecting and Scaling Ground Motion Time Histories According to Eurocode 8 and ASCE 7-05. Earthquakes and Structures, 5(2), 129-142.

[34] Zuboski, G.R. (2013). Stress-Strain Behavior for Actively Confined Concrete Using Shape Memory Alloy Wires. Thesis Presented in Partial Fulfillment of the Requirements for the Degree Master of Science .Graduate School of The Ohio State University.

[35] Mazars, J., & Grange, S. (2015). Modeling of Reinforced Concrete Structural Members for Engineering Purposes. Computers and Concrete, 16(5), 683-701.

[36] Panagiotakos, T. B., & Fardis, M. N. (2001). Deformations of Reinforced Concrete Members at Yielding and Ultimate. Structural Journal, 98(2), 135-148.

[37] Shome, N., Cornell, C. A., Bazzurro, P., & Carballo, J. E. (1998). Earthquakes, Records, and Nonlinear Responses. Earthquake Spectra, 14(3), 469-500.

[38] PEER, Pacific Earthquake Engineering Research Center. (2015). http://peer.berkeley.edu/nga.

[39] Vamvatsikos, D., & Cornell, C. A. (2002). Incremental Dynamic Analysis. Earthquake Engineering & Structural Dynamics, 31(3), 491-514.

[40] Haselton, C. B., Liel, A. B., & Deierlein, G. G. (2009). Simulating structural collapse due to earthquakes: model idealization, model calibration, and numerical solution algorithms. Computational methods in structural dynamics and earthquake engineering (COMPDYN).